Magnetic Resonance Assessment of RV Remodeling and Function

10

Lars Grosse-Wortmann and Adam L. Dorfman

Abstract

Cardiac magnetic resonance imaging (CMR) provides unique opportunities for the assessment of right ventricular (RV) geometry, function, and myocardial structure. These allow CMR to play a pivotal role in diagnosis, monitoring, and decision-making in pediatric and congenital cardiology. CMR is the reference standard for quantification of RV volume, ejection fraction and mass. Phase contrast flow velocity mapping by CMR offers an accurate measurement of pulmonary blood flow and of the degree of pulmonary regurgitation in the presence of pulmonary valvar insufficiency, for example after Tetralogy of Fallot repair. More recently, CMR has been employed for the quantification of RV strain, rotation, and torsion. CMR allows for the complete visualization of the RV as compared to echocardiography, but is hampered by inferior temporal resolution, particular for the assessment of diastolic function. Scar imaging with late gadolinium enhancement CMR is established as a risk predictor in certain types of congenital and acquired heart disease, although it can be difficult to detect scarring with certainty in the thin walled RV myocardium. For the same reason, the assessment of diffuse myocardial fibrosis in the RV by CMR T1 mapping is challenging.

In this chapter we describe the technical underpinnings of CMR for the RV, outline its utility and limitations in pediatric and congenital heart disease, and provide examples on how CMR contributes to clinical decision making.

L. Grosse-Wortmann (✉)
Paediatric Cardiology, Labatt Family Heart Centre, Hospital for Sick Children, 555 University Ave, Toronto, ON M1G 1X8, Canada
e-mail: lars.grosse-wortmann@sickkids.ca

A.L. Dorfman
University of Michigan, Congenital Heart Center, Department of Pediatrics, C.S. Mott Children's Hospital, University of Michigan, 1540 E. Hospital Drive, Ann Arbor, MI 48109, USA

Introduction

One of the pivotal strengths of cardiac magnetic resonance imaging (CMR) is the ability to accurately and reproducibly quantify the size and function of the right ventricle (RV) [1]. Using techniques that include standard cine imaging, myocardial deformation and tissue characterization, CMR affords novel insights into the structure, myocardial composition, and function of the RV. In clinical practice, CMR has become the gold standard for quantification of RV volumes and ejection fraction. This asset is of enormous clinical importance in the care of patients with congenital as well as acquired pediatric heart disease. For example, in repaired tetralogy of Fallot (rTOF) and pulmonary hypertension (PHTN), RV size, ejection fraction, and mass by CMR have been linked to outcomes and aid in clinical decision-making [2–4].

Imaging Techniques for Assessing RV Size and Ejection Fraction

The current CMR technique of choice for the quantification of RV size and systolic function is by cine imaging using steady state free precession techniques (SSFP, Fig. 10.1; Videos 10.1a and 10.1b). A variety of modifications, including
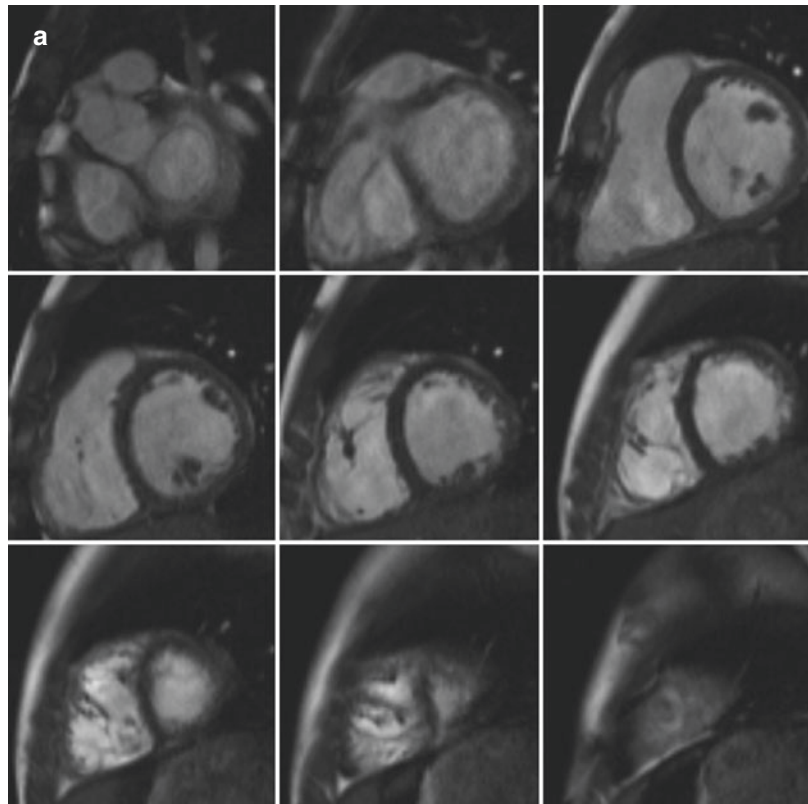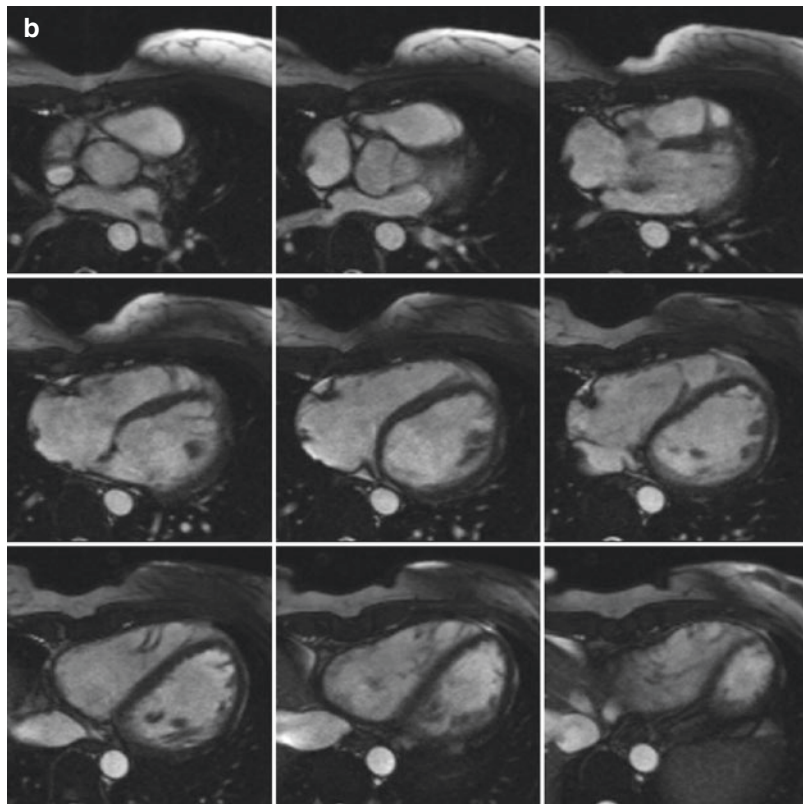

Fig. 10.1 Short axis (**a**) and axial stack (**b**) of steady state free precession images at end-diastole in a patient with Tetralogy of Fallot. See also Videos 10.1a and 10.1b

Fig. 10.1 (continued)

parallel imaging and partial Fourier imaging, are routinely applied to accelerate the imaging acquisition, allowing for shorter breathhold durations. The temporal resolution should be adjusted to allow for at least 20–25 true images per cardiac cycle, not through interpolation. Decreasing temporal resolution results in faster imaging time but risks missing the true maximum and minimum ventricular volumes at end- diastole and -systole, respectively.

For RV volumetry, a stack of parallel slices is acquired that cover the ventricle. Theoretically, this can be done in any plane, as long as the entire ventricle is included. In clinical practice, the RV is measured from either a short axis stack or an axial stack of images. Some studies have found that measuring the RV in the axial plane has better reproducibility [5] while others showed no significant difference between the orientations [6], and both approaches remain in wide clinical use. In contrast to ventricular volume measurements by echocardiography, cine CMR is not a real time technique; end-systole and end-diastole are not defined based on ECG, but on the smallest and largest ventricular sizes, respectively. By this definition, in patients with rTOF, who typically have complete right bundle branch block, RV end-systole often occurs later than LV end-systole due to delayed RV activation.

During post-processing, the area encompassed by the RV endocardium is quantified in each slice, by manually tracing the endocardial-blood pool border. This area is multiplied by the sum of the slice thickness and gap between slices, using the method of disks. No assumptions are made about the RV luminal area, as opposed to Simpson's method in echocardiography, which is based on the RV diameter in one or two dimensions. However, contouring the endocardial-blood border in the heavily trabeculated RV can be challenging (Fig. 10.2a), as numerous muscle bundles cannot practically be excluded from the blood pool and are therefore included in the ventricular volume rather than in its mass. Alternatively, it is
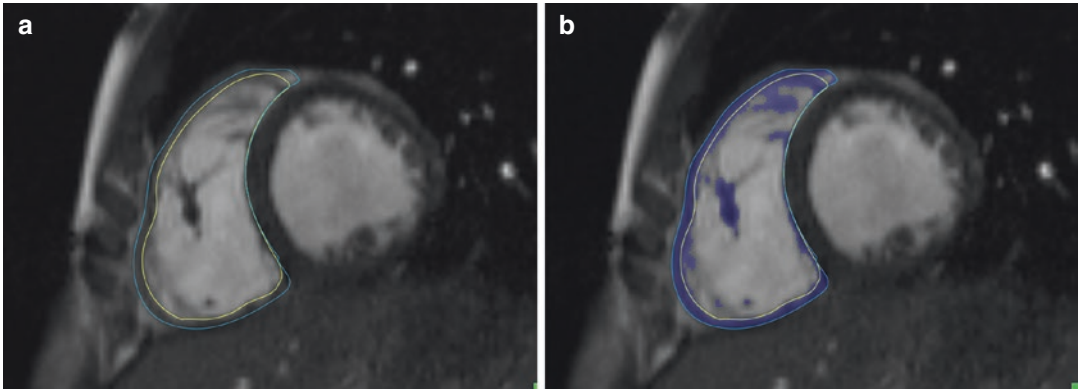
Fig. 10.2 Postprocessing of right ventricular volume and mass in short axis at end-diastole. The endocardial border can be defined either by contouring (**a**, *yellow line*) or by thresholding (**b**). Note how by thresholding the trabeculations in the right ventricular cavity are included in the muscle mass

possible to detect myocardium by applying 'thresholding' (Fig. 10.2b), via signal intensity differences between the blood pool and the myocardium. Using this approach, even complex trabeculations are readily included in the ventricular mass. However, measurements performed with thresholding differ from published normative data, most of which were generated using the classic contouring techniques, so that new normative data sets are necessary.

The greatest variability in the quantification of RV volumes is introduced by contouring slices around the tricuspid and pulmonary valve annuli. A cine stack in the axial orientation is more 'vulnerable' to inaccuracies around the pulmonary valve, while it is more difficult to identify the border between atrium and ventricle in the short axis orientation. Neither the tricuspid nor the pulmonary valve annulus is entirely 'flat' and, therefore, part of the imaging slice will be on the 'ventricular side' while part will be on the 'atrial side'. Nonetheless, in the short axis orientation the imaging plane should be prescribed as parallel to the valve annulus as possible, using the double oblique technique [6, 7]. In addition, most quantification software packages offer a cross-referencing function, in which the location of the short axis slice can be visualized in the vertical and horizontal long axis cine images and vice versa. Identifying the location of the pulmonary valve annulus can be particularly difficult in individuals with rTOF, particularly after transannular

patch repair when there is little residual pulmonary valve tissue to visualize. In this case, knowledge of the anatomy, including the expected location of the pulmonary annulus, is helpful in obtaining accurate measurements.

There are several published sets of normative data for RV size and ejection fraction [8–11]. However, all such data in children are limited by low sample sizes. For smaller children who typically require sedation or anesthesia for MRI scanning normal values are nearly absent [9]. When using a normative dataset for comparison, it is important to ensure that scanning and postprocessing techniques are similar (e.g.; axial vs. short axis imaging for RV volumetry, use of sedation, contouring vs. thresholding) and that the patient population is consistent with that in the reference used (e.g.; age, gender).

In general, 2-D echo measurements of the RV do not correlate well with volume measurements by CMR [12]. There are a number of reasons for this discrepancy, including the fact that most echocardiographic metrics of RV systolic function are based on longitudinal shortening in the inlet and apical trabecular portions. Many patients with rTOF, for example, have a dysfunctional infundibulum, which these methods do not capture (Fig. 10.3). 3-D echo has been more promising, with better correlation but consistent underestimation of right ventricular volume compared to CMR, both in congenital heart disease and other disease states [13, 14]. Knowledge-
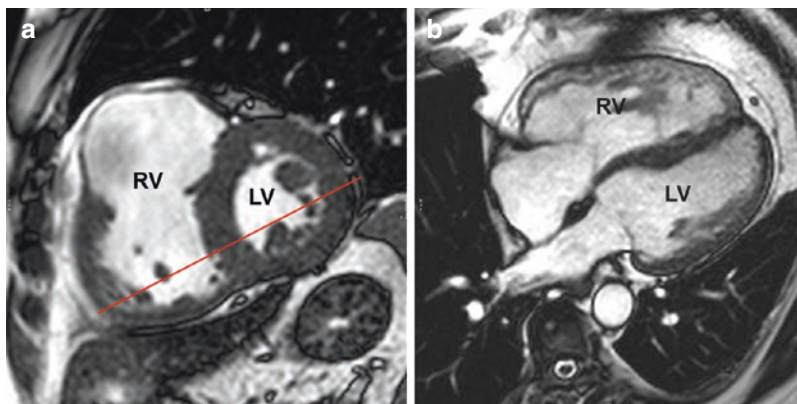
Fig. 10.3 Cardiac magnetic resonance steady state free precession image of the right and left ventricles in short axis (**a**) and four chamber view (**b**). The right ventricle is dilated. Note the dilated and thin anterior wall of the infundibulum. The *red line* on the short axis image delineates the four chamber plane. Note that the four chamber view does not include the dyskinetic infundibulum. *LV* left ventricle, *RV* right ventricle

based reconstruction of 2-D echo data into a 3-D data set, using pre-defined landmarks and a 'library' of lesion-specific RV shapes, has been compared to CMR in rTOF patients with good reproducibility and good correlation of volume measurements [15].

Exact quantification of RV size and volumes is important in a variety of congenital heart lesions, most commonly in TOF, where RV volumes feature prominently both in risk prediction and in decision making regarding timing of pulmonary valve replacement [16–19]. Other types of congenital heart disease in which CMR volumetry is commonly applied include functionally single ventricles with a dominant RV [20], subsystemic RVs in transposition of the great arteries [21] and Ebstein's anomaly of the tricuspid valve [22]. In addition, CMR measurement of RV ejection fraction in pediatric pulmonary hypertension is predictive of survival [3]. In arrhythmogenic right ventricular cardiomyopathy, RV ejection fraction and end-diastolic volume are criteria in the diagnostic score [23, 24].

Regional and Compartmental Function of the Right Ventricle

While ejection fraction provides a useful gauge for global systolic function, regional variations in contractility have pathophysiological, diagnostic, and even prognostic significance. In ARVC for example [24], a positive imaging criterion is conditional on the presence of regional wall motion abnormalities (RWMAs) within the RV. In a recent study of children under investigation for ARVC [23], patients with greater certainty for ARVC as per the revised Task Force Criteria [24] were not only more likely to have RWMAs, but also had more severe RWMAs. Diagnosing subtle RWMAs, even with the superior visualization of the anterior wall of the RV provided by CMR, is challenging, with considerable interobserver variability [23].

The abilities of CMR to cover the entire heart and depict RV geometry and function without geometric assumptions make it an ideal tool for the description of RV compartmental function. The normal RV is composed of an inlet portion, an apical trabecular portion, and an outlet. Global RV dysfunction can be the result of (1) homogenous hypocontractility of all of these segments, (2) hypo- or akinesia of one of the segments, or (3) dyssynchrony. Conversely, RV ejection fraction can be preserved even in the presence of dysfunction of one of its components. In contrast to the left ventricle, there is no universally accepted method for segmentation of the RV. Wald et al. proposed to divide the RV into ten segments [25], although the segment boundaries are not well established by anatomical landmarks in their model. Zhong and co-workers [26] introduced a 13-segment model of the RV. Most

studies, however, particularly in TOF, do not use a segmental approach, but merely differentiate an outlet or infundibular portion from the remainder of the RV, sometimes referred to as the RV sinus. As pointed out above, the distal RV outflow tract in rTOF is often grossly dilated and dyskinetic, while the inferior wall and inlet portions of the RV contract normally [27, 28]. The resultant ejection fraction of an RV with aneurysmal outflow tract can be the same as that of a ventricle with global dysfunction and normal sized outflow tract. In patients with a very dyskinetic RVOT, global RV ejection fraction measured by CMR can be up to 25% lower as compared to a normally functioning RVOT [29]. Most rTOF patients in the current surgical era have preserved RV function outside of the outflow tract. Whether or not the function of the RVOT or that of the remainder of the RV is of greater significance for the patient's clinical status after TOF repair is under debate. Wald et al. found that RVOT ejection fraction was the only RV parameter that was associated with aerobic capacity as a surrogate of clinical well-being [25]. In contrast, Bove and Alghamdi and their respective co-workers described a closer association between ejection fraction of the RV 'sinus' portion [30] and RV longitudinal shortening [29] and peak oxygen uptake (VO_{2max}) during exercise than between global RV or RVOT ejection fraction and VO_{2max}.

In Ebstein anomaly of the tricuspid valve, RV longitudinal function is typically preserved and sometimes even supranormal [31]. As compared to a normal heart, the apical region contributes relatively more to global systolic function.

Imaging Techniques for Assessing Pulmonary Regurgitation

Pulmonary flow and regurgitation are measured using phase contrast (PC MRI) flow velocity mapping in the main pulmonary artery. Quantification of pulmonary regurgitation is part of the routine CMR examination in patients with repaired rTOF. The authors suggest PC MRI be performed during free breathing, since breath holding can alter pulmonary blood flow [32]. Pulmonary regurgitation can be expressed as a percentage of systolic forward flow, or "regurgitant fraction" (Fig. 10.4), or as an absolute volume of retrograde flow per beat or per minute. Pulmonary regurgitant volume appears to be a better correlate of RV volume than regurgitant fraction [33, 34].

There are important pitfalls to PC MRI: For example, turbulent flow from RV outflow tract obstruction can result in underestimation of volume and velocity of flow [35]. Newer 4-D PC MRI sequences allow for flexibility in choosing an area of the vessel that has less turbulence and lower velocity of flow. Currently a research tool, it is expected that 4D PC MRI sequences will be part of the clinical armamentarium in the near future (Fig. 10.5; Video 10.2). Underestimation of flow volume in dilated pulmonary arteries is a widely recognized problem. This may be in part due to helical flow patterns and vortex formation [36] and to translational motion of the main pulmonary artery through the imaging plane in the presence of significant pulmonary regurgitation. In some situations it may be more accurate to measure flows in both branch pulmonary arteries and use their sum as a proxy for main pulmonary artery flow, unless there is isolated unilateral PA flow reversal [37].

Imaging Techniques for Assessing Myocardial Deformation

Myocardial strain, measures the local change in length or thickness of a myocardial segment through the cardiac cycle, expressed as a percentage change. The components of strain include circumferential, longitudinal and radial deformation. If the myocardium shortens from diastole to systole, as occurs in the circumferential and longitudinal directions, the strain is described as a negative number, with a higher

Fig. 10.4 Flow curve obtained from phase contrast imaging through the main pulmonary artery. This patient has severe pulmonary regurgitation, as evidenced by the negative flow seen after 340 ms on the x-axis
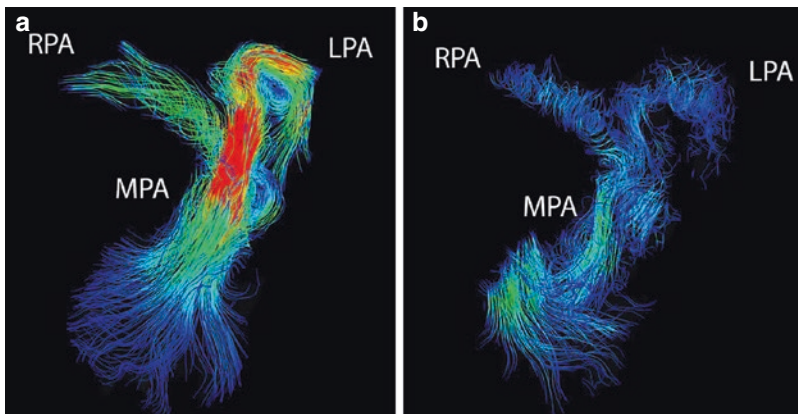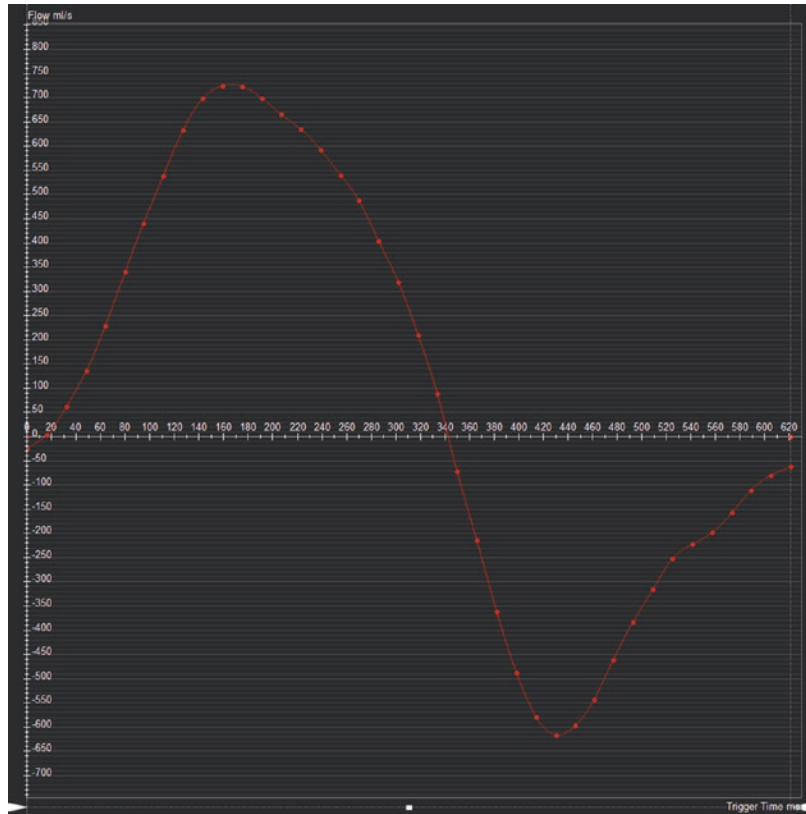

Fig. 10.5 Four-dimensional phase contrast imaging in a patient with Tetralogy of Fallot, depicting the streamlines of flow during systole (**a**) and diastole (**b**). Note the flow acceleration in the right ventricular outflow tract during systole and flow reversal during diastole (images and movie courtesy of M. Rose, M. Markl, J. Robinson, C. Rigsby, Northwestern University, Chicago, IL). *LPA* left pulmonary artery, *MPA* main pulmonary artery, *RPA* right pulmonary artery. See also Video 10.2

magnitude equating to greater strain. In the radial direction, the myocardium thickens in systole, leading to a positive strain value. Strain can be described from a Lagrangian or Eulerian perspective. While an extended discussion of this concept is beyond the scope of this chapter, the values differ and it is important to recognize which type of data is being measured by a given software package.

The right ventricle poses particular challenges, mostly related to the thin free wall and the more complex geometry, compared to the bullet-shaped, thicker walled, LV. There are several CMR-based techniques for measuring myocardial strain in either the right or left ventricle. These approaches can be compared to tissue Doppler and speckle-tracking strain imaging by echocardiography. In general, these techniques offer better temporal resolution than CMR. However, echo remains dependent on acoustic windows, and CMR offers more consistent and superior visualization of all segments of the heart, especially the RV [38, 39].

The most established method for measuring myocardial strain by CMR is with tagged images. This is accomplished with a sequence using spatial modulation of magnetization (SPAMM), resulting in a grid that is laid on top of the myocardium (Fig. 10.6; Video 10.3). This grid deforms with the myocardium throughout the cardiac cycle. Post-processing software is used track this deformation to obtain measurements of strain. Short axis images are used to analyze circumferential and radial strain, and long axis images to analyze longitudinal strain. However, the tag line spacing is typically at least 6–8 mm, making this technique of limited use for analyzing the thin RV free wall.

Sensitivity-encoded MRI (SENC) is another tagging-based sequence for measurement of strain that has been used more successfully for analysis of the RV [40, 41]. Unlike traditional tagging sequences, the SENC tags are generated in the through-plane, so that short axis images are used to measure longitudinal strain, and long axis images to measure circumferential strain.

The spatial resolution for strain analysis is the same as the imaging voxel size, which is why SENC is a more viable technique for RV strain analyses.

In DENSE (displacement encoding with stimulated echoes), as for traditional tagging, SPAMM is used to encode the position of myocardium throughout the cardiac cycle. However, DENSE provides phase-reconstructed images that encode displacement at a voxel-level resolution of strain data (Fig. 10.7) [42]. A 3D DENSE sequence has been developed more recently, which may be of additional benefit for measuring the complex deformation patterns of the right ventricle [43].

As for SPAMM-based tagging sequences, both SENC and DENSE require the acquisition of specific sequences while the patient is in the scanner. Feature-tracking, on the other hand, generates strain data using SSFP cine images. Thus, no additional sequences are required and data can be analyzed retrospectively, using the short axis
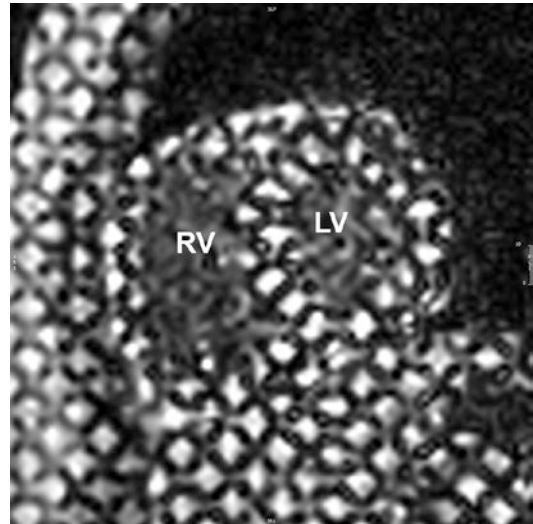

Fig. 10.6 Tagged short axis CMR image. The grid superimposed on the heart deforms with the myocardium through the cardiac cycle. Note that the spacing between the tag lines is wider than the free wall of the right ventricle, limiting the use of CMR tagging for analysis of right ventricular mechanics. *LV* left ventricle, *RV* right ventricle. See also Video 10.3
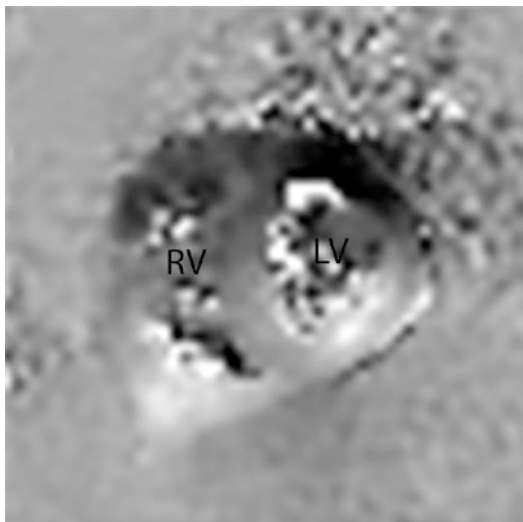
Fig. 10.7 Two-dimensional cine displacement-encoded MR (DENSE) phase image in the short axis plane. Displacement is encoded into the phase of each voxel, providing high spatial resolution that is necessary for measuring RV strain (image courtesy of M. Fogel, Philadelphia, PA). *LV* left ventricle, *RV* right ventricle

stack that was acquired for ventricular volumetry (for circumferential and radial strain) as well as two- and four-chamber cine sequences (for longitudinal strain) (Fig. 10.8) [44].

Right ventricular myocardial deformation imaging with the techniques described above (tagging, SENC, DENSE, feature tracking) has been applied predominantly in the rTOF population, in the hope that changes in strain may be an earlier finding of compromised RV 'health' than size or ejection fraction, providing an opportunity for more timely pulmonary valve replacement before irreversible damage to the RV occurs [45–47]. Right ventricular longitudinal strain has been shown to be a predictor of adverse outcome in this population, independent of ventricular size or ejection fraction [48].
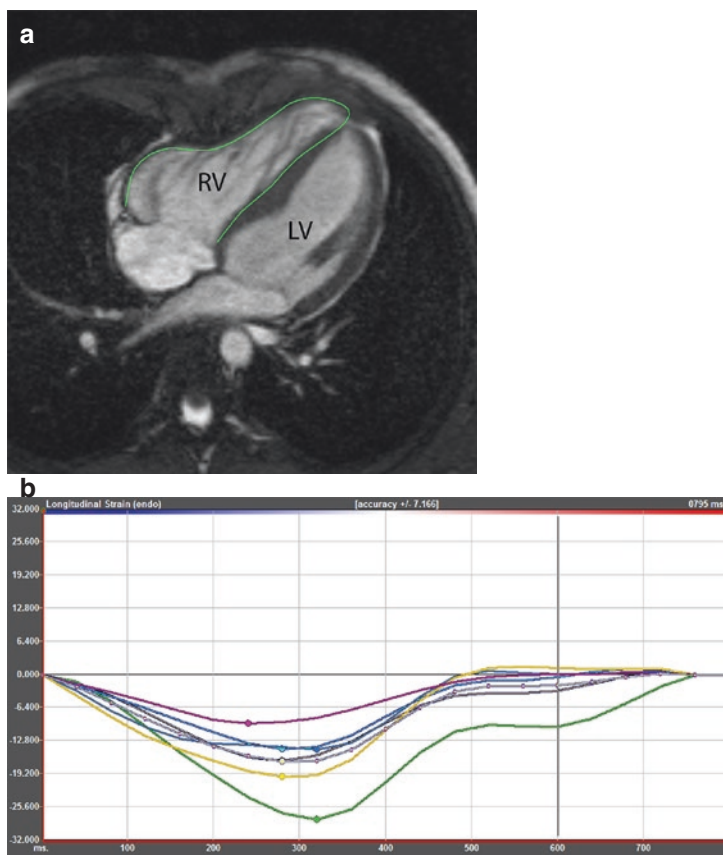
Fig. 10.8 Cardiac magnetic resonance feature tracking analysis in a patient with repaired tetralogy of Fallot, based on routine steady state free precession cine images (**a**), similar to Figure 10.3. Using the endocardial contour through-out the cardiac cycle and a proprietary analysis algorithm, the software derives segmental RV longitudinal strain curves (**b**). LV=left ventricle, RV=right ventricle. See supplemental material for movie file

Imaging Techniques for Assessing Myocardial Scarring and Fibrosis

Detection and Quantification of Fibrosis with CMR

The detection and quantification of myocardial scar and diffuse fibrosis is one of the unique assets of CMR. Discrete scars surrounded by relatively healthy myocardium are detected by late gadolinium enhancement (LGE) imaging. Late gadolinium enhancement CMR is based on different wash in and washout kinetics of gadolinium contrast in healthy vs. scarred myocardium: In the absence of scarring, gadolinium is rapidly taken up, but also quickly cleared from the myocardium, within a matter of minutes. In scarred tissue, gadolinium becomes trapped within the fibrous strands of the extracellular matrix. Similar to chronic scars, acute necrosis, either through infarction or inflammation, also produces LGE, presumably due to gadolinium trapping within necrotic tissue and ruptured myocytes [49]. LGE sequences are T1 weighted, showing gadolinium deposits as signal intense regions. The size of these regions can be quantified and expressed as a percentage of the total myocardium.

Importantly, LGE relies on a critical scar size for detection as well as on the contrast between healthy and diseased myocardium. Hence, if the myocardium is uniformly fibrosed or if the scars are very small, LGE imaging may be falsely reassuring as this technique is 'blind' to diffuse fibrosis. T1 relaxometry, often referred to as 'T1 mapping,' is a quantitative approach which exploits the differences in tissue specific longitudinal relaxation (or T1 recovery) kinetics (Fig. 10.9; Video 10.4). Fibrosed myocardium has higher T1 times as compared to healthy myocardium. Using pre- and post-contrast T1 time measurements, as well as the patient's hematocrit, the extracellular volume (ECV) can be quantified as an approximation of the patient's extracellular matrix, relative to the total myocardial volume (within an imaging voxel). It must be noted that the overlap of native T1 times and of ECV between health and disease is significant, limiting its use in identifying pathology.
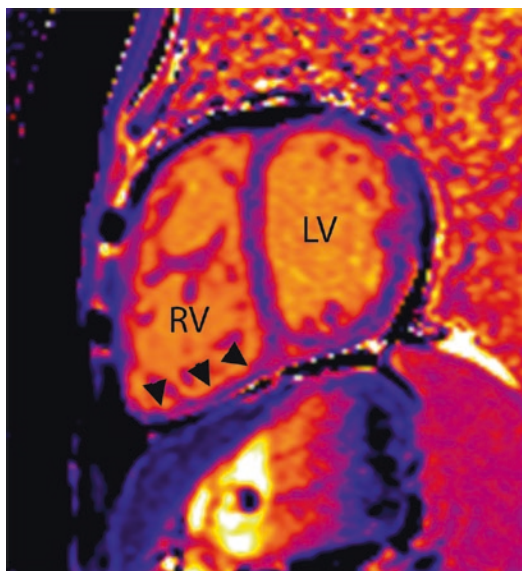

Fig. 10.9 Non-contrast T1 map in a patient with repaired tetralogy of Fallot. Each color encodes for a specific T1 time. Higher T1 times are found in fibrotic myocardium. Note the thin RV diaphragmatic (arrowheads) and free walls, making it difficult to draw a region of interest that excludes the blood pool as well as epicardial fat. *LV* left ventricle, *RV* right ventricle

Nevertheless, T1 relaxometry has provided important insights into pathophysiology and is expected to become useful during serial monitoring when followed within the same patient.

While a wealth of science and clinical experience is available on LV fibrosis imaging using LGE and T1 relaxometry, the understanding of RV fibrosis and its significance is limited. The reasons for the paucity of data include not only a scientific focus on the LV, particularly in acquired heart disease, but also the technical challenges of 'fibrosis imaging' in the RV. The finite spatial resolution of LGE CMR sequences and partial volume effects (combining the signal properties of two adjacent tissues) with blood and epicardial fat render scar imaging in the RV challenging [50]. In fact, in cases of confirmed RV infarction the sensitivity of LGE to identify necrotic myocardium was only 16% [51]. Some experts advocate for the acquisition of LGE at end-systole when the myocardium is thicker and the LGE less prone to partial volume effects between myocardium and blood. The accuracy of CMR
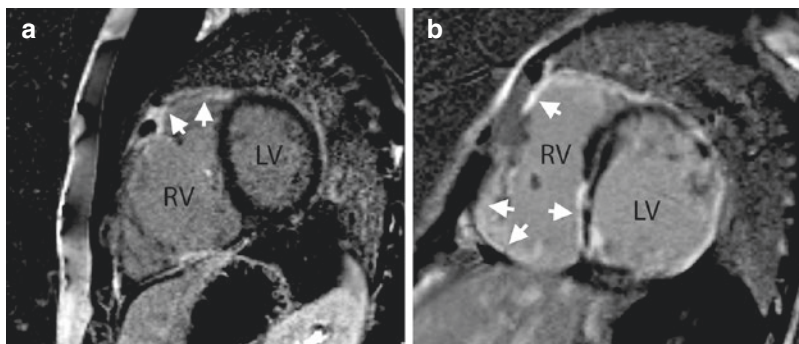
Fig. 10.10 Late gadolinium enhancement imaging in short axis orientation in (**a**) a patient with Ebstein anomaly of the tricuspid valve and (**b**) a patient with arrhythmogenic right ventricular cardiomyopathy with severe biventricular involvement. Arrows denote areas of right ventricular scarring, as evidenced by the retention of gadolinium, giving high signal intensity on T1 weighted imaging. *LV*=left ventricle, *RV*=right ventricle

sequences for native T1 and ECV measurements in the RV is a topic of debate. One of the challenges of T1 relaxometry is that the maximum spatial resolution of most sequences approaches the myocardial thickness of the RV. As each 'T1 map' contains the composite information from several (typically 5–11) 'source' images, T1 quantification also relies on the co-registration of these images. Both the limited spatial resolution relative to the RV thickness and imperfect image registration can lead to partial volume effects between myocardium and blood. As a result, measurements of the myocardium are 'contaminated' by blood falsely elevating T1 and ECV. Nevertheless, a recent T1 mapping study in patients after TOF repair reported values in the RV inferior wall and outflow tract with reasonable reproducibility [52]. Experimental approaches using segmented k-space sampling, i.e. collecting the imaging data over multiple heartbeats, rather than single shot techniques which use the information from a single heart beat to reconstruct the entire image, have shown promise in measuring RV T1 times [53].

Overall, evidence is accumulating that RV myocardial fibrosis, both diffuse and patchy, is present in many patients with congenital heart disease (Figure 10.10a), particularly in those with increased afterload such as pulmonary hypertension [54] and in RV hypoplasia [55]. There is early evidence that surgical factors play a role in the development of fibrosis [56].

Residual lesions also seem to be important [52]. However, we do not yet understand the exact pathophysiological triggers, nor do we know when fibrosis manifests and how it progresses. Some patients with congenital heart disease appear to have a profibrotic milieu, with an augmented collagen metabolism, which is associated with greater degrees of RV LGE by CMR [57]. A certain genetic make-up and epigenetic phenomena also appear to promote fibrosis [58].

In a study of adults after atrial redirection surgery for transposition of the great arteries, half had myocardial scarring by LGE in their systemic right ventricles [59, 60]. The presence of LGE was associated with electromechanical delay and ventricular dyssynchrony, as well as with atrial arrhythmias. One patient had progression in the amount of LGE during follow-up, suggesting that scarring is not static, but can worsen over time. Adults after the atrial switch procedure also have increased ECV within the interventricular septum, although the clinical significance of this finding has yet to be demonstrated [61]. Although the long-term cardiac health after the arterial switch operation appears to be better than with the atrial switch procedures, T1 mapping data in children and adolescents after arterial switch suggests an increased level of diffuse myocardial fibrosis (Grotenhuis, *unpublished data*).

Patchy scarring within the RVOT is an inevitable consequence of surgical RV reconstruction as part of the TOF repair. Not surprisingly, LGE

within the RVOT is associated with dyskinesia of that compartment of the RV [25]. The ventricular septal defect patch also enhances routinely. In a study of 92 TOF patients, Babu-Narayan et al. found LGE in these regions in nearly every patient [62]. However, one fourth also had LGE outside of the patch and the RVOT. The mechanism of LGE in these locations is less clear and has been interpreted as a sign of chronic remodeling rather than surgical trauma. These patients were older, had later repair, and had higher RV end-systolic volume. Patients with a greater RV LGE extent were more likely to experience arrhythmias and have decreased exercise tolerance. In another study, Park et al. showed that the extent of RV LGE was associated with fragmentation of the electrocardiogram QRS complex, which signifies conduction abnormalities and predisposes to arrhythmias [63]. Importantly, most patients in these two studies had been operated in the 1970s and 1980s. Clinical experience indicates that for patients who underwent operation in the current surgical era, LGE outside of the predilection sites is rare, suggesting overall healthier RV myocardium.

Two recent studies in adults with TOF found elevated RV ECV in patients with TOF as compared to controls [52, 64]. In one of them, greater RV ECV was associated with female gender and lower RV mass-to-volume ratio. Patients with predominant RV volume overload as opposed to pressure overload had higher ECV. A subsequent study in children, using native T1 as a CMR marker of fibrosis, also found evidence of increased RV fibrosis in TOF patients and confirmed the associations with volume overload [65].

An increased degree of myocardial fibrosis and RV wall thinning [66] has also been recognized in cardiomyopathic diseases (Figure 10.10b). In arrhythmogenic right ventricular cardiomyopathy (ARVC), for example, fibrofatty replacement diagnosed by histology during endomyocardial biopsy or pathology is part of the revised Task Force Criteria for the diagnosis of this condition. CMR, using LGE and T2 weighted turbo spin echo sequences, has been proposed as a noninvasive tool for the detection of fibrotic changes and fatty remodeling of RV myocardium. However, the ability of RV LGE to detect scarring in ARVC has been questioned in clinical practice. In a study of 142 pediatric patients who were evaluated for ARVC, including 23 with 'definite' ARVC, only three patients had evidence of RV scarring by LGE [23]. Importantly, all three had other signs of myocardial pathology, including global and regional RV dysfunction so that the added clinical benefit from a positive LGE result was incremental.

Myocardial Viability

Healthy myocardium contracts and thickens with every heartbeat. With the exception of intrinsic myopathic processes (not covered in detail here), reduced myocardial contractility reflects an imbalance between myocardial substrate demand and supply. This imbalance manifests in coronary ischemia, most often as a result of coronary artery stenosis, compression, or thromboembolism; or caused by low cardiac output or inadequate blood pressure. Reduced myocardial contractility at rest is a sign of severely compromised myocardial perfusion. In patients with preserved contractility at rest, a supply/demand deficit may be unmasked by increasing the myocardial oxygen requirement. This is accomplished with either exercise [67] or pharmacological 'stress', most often using dobutamine. The physiologic response to both exercise and dobutamine administration is an increase in heart rate, ejection fraction, and stroke volume, via a decrease in RV end-systolic volume.

An abnormal RV stress CMR is often characterized by a less than normal decrease in RV end-systolic volume, resulting in a blunted increase in ejection fraction. Such a response to exercise can identify endurance athletes who are at risk for ventricular arrhythmias [68]. In some patients after TOF repair, the RV end-systolic volume by CMR during dobutamine infusion fails to

decrease, or even increases; this pathologic finding is usually not predictable from examination at rest [69]. Similarly, many patients after TOF repair do not respond to exercise with an increase in RV ejection fraction [70]. A weaker increase in RV ejection fraction with dobutamine predicts a steeper decline in exercise tolerance during follow-up [71]. Fontan patients, and especially those with dominant RVs, respond with an increase in ejection fraction to low dose dobutamine stress [72].

'Stress CMR' also provides clues to the presence of RV diastolic dysfunction: In TOF, an infusion of low dose dobutamine at a concentration of 7.5mcg/kg/min reveals abnormal RV relaxation. In a study of patients after atrial switch operation for transposition of the great arteries, an infusion of dobutamine leads to an increase in RV contractility, but not to an augmentation in cardiac output [73]. The authors concluded that RV filling did not increase enough to provide the preload necessary to support an increase in cardiac output. Interestingly, patients after atrial switch do not increase their RV ejection fraction with exercise and experience regional wall motion abnormalities at rest and exercise [74].

First pass gadolinium perfusion CMR is widely used to assess LV myocardial viability in coronary artery disease, but also in patients with anomalous coronary artery origins, after coronary artery transfer, or with Kawasaki disease. In conjunction with myocardial deformation and LGE it can help differentiate between scarred (impaired contractility, reduced perfusion, positive LGE), hibernating (impaired contractility, reduced perfusion, but no LGE), and stunned myocardium (impaired contractility, normal perfusion, no LGE). However, the evaluation of first pass perfusion of the thin-walled subpulmonic RV with CMR is challenging due to the limited spatial resolution of commercially available sequences and not undertaken in clinical practice. First pass perfusion of the hypertrophied systemic RV may be more feasible, but no published data are available.

References

1. Mooij CF, de Wit CJ, Graham DA, Powell AJ, Geva T. Reproducibility of MRI measurements of right ventricular size and function in patients with normal and dilated ventricles. J Magn Reson Imaging. 2008;28(1):67–73.

2. Geva T. Repaired tetralogy of Fallot: the roles of cardiovascular magnetic resonance in evaluating pathophysiology and for pulmonary valve replacement decision support. J Cardiovasc Magn Reson. 2011;13:9.

3. Moledina S, Pandya B, Bartsota M, et al. Prognostic significance of cardiac magnetic resonance imaging in children with pulmonary hypertension. Circ Cardiovasc Imaging. 2013;6(3):407–14.

4. Valente AM, Gauvreau K, Assenza GE, et al. Contemporary predictors of death and sustained ventricular tachycardia in patients with repaired tetralogy of Fallot enrolled in the INDICATOR cohort. Heart. 2014;100(3):247–53.

5. Clarke CJ, Gurka MJ, Norton PT, Kramer CM, Hoyer AW. Assessment of the accuracy and reproducibility of RV volume measurements by CMR in congenital heart disease. JACC Cardiovasc Imaging. 2012;5(1):28–37.

6. D'Errico L, Lamacie MM, Jimenez Juan L, et al. Effects of slice orientation on reproducibility of sequential assessment of right ventricular volumes and ejection fraction: short-axis vs transverse SSFP cine cardiovascular magnetic resonance. J Cardiovasc Magn Reson. 2016;18(1):60.

7. Grosse-Wortmann L, Lee W, Yoo SJ. Magnetic resonance imaging and computed tomography. In: Anderson R, Baker E, Penny D, Redington A, Rigby M, Wernovsky G, editors. Paediatric cardiology. Philadelphia, PA: Churchill-Livingstone; 2009. p. 363–78.

8. Alfakih K, Plein S, Thiele H, Jones T, Ridgway JP, Sivananthan MU. Normal human left and right ventricular dimensions for MRI as assessed by turbo gradient echo and steady-state free precession imaging sequences. J Magn Reson Imaging. 2003;17(3):323–9.

9. Buechel EV, Kaiser T, Jackson C, Schmitz A, Kellenberger CJ. Normal right- and left ventricular volumes and myocardial mass in children measured by steady state free precession cardiovascular magnetic resonance. J Cardiovasc Magn Reson. 2009;11:19.

10. Robbers-Visser D, Boersma E, Helbing WA. Normal biventricular function, volumes, and mass in children aged 8 to 17 years. J Magn Reson Imaging. 2009;29(3):552–9.

11. Sarikouch S, Peters B, Gutberlet M, et al. Sex-specific pediatric percentiles for ventricular size and mass as reference values for cardiac MRI: assessment by steady-state free-precession and phase-contrast MRI flow. Circ Cardiovasc Imaging. 2010;3(1):65–76.

12. Lai WW, Gauvreau K, Rivera ES, Saleeb S, Powell AJ, Geva T. Accuracy of guideline recommendations for two-dimensional quantification of the right ventricle by echocardiography. Int J Cardiovasc Imaging. 2008;24(7):691–8.

13. Crean AM, Maredia N, Ballard G, et al. 3D Echo systematically underestimates right ventricular volumes compared to cardiovascular magnetic resonance in adult congenital heart disease patients with moderate or severe RV dilatation. J Cardiovasc Magn Reson. 2011;13:78.

14. Nagata Y, Wu VC, Kado Y, et al. Prognostic value of right ventricular ejection fraction assessed by transthoracic 3d echocardiography. Circ Cardiovasc Imaging. 2017;10(2):pii: e005384.

15. Dragulescu A, Grosse-Wortmann L, Fackoury C, et al. Echocardiographic assessment of right ventricular volumes after surgical repair of tetralogy of Fallot: clinical validation of a new echocardiographic method. J Am Soc Echocardiogr. 2011;24(11):1191–8.

16. Buechel ER, Dave HH, Kellenberger CJ, et al. Remodelling of the right ventricle after early pulmonary valve replacement in children with repaired tetralogy of Fallot: assessment by cardiovascular magnetic resonance. Eur Heart J. 2005;26(24):2721–7.

17. Knauth AL, Gauvreau K, Powell AJ, et al. Ventricular size and function assessed by cardiac MRI predict major adverse clinical outcomes late after tetralogy of Fallot repair. Heart. 2008;94(2):211–6.

18. Oosterhof T, van Straten A, Vliegen HW, et al. Preoperative thresholds for pulmonary valve replacement in patients with corrected tetralogy of Fallot using cardiovascular magnetic resonance. Circulation. 2007;116(5):545–51.

19. Therrien J, Provost Y, Merchant N, Williams W, Colman J, Webb G. Optimal timing for pulmonary valve replacement in adults after tetralogy of Fallot repair. Am J Cardiol. 2005;95(6):779–82.

20. Rathod RH, Prakash A, Kim YY, et al. Cardiac magnetic resonance parameters predict transplantation-free survival in patients with fontan circulation. Circ Cardiovasc Imaging. 2014;7(3):502–9.

21. van der Bom T, Winter MM, Bouma BJ, et al. Effect of valsartan on systemic right ventricular function: a double-blind, randomized, placebo-controlled pilot trial. Circulation. 2013;127(3):322–30.

22. Hosch O, Sohns JM, Nguyen TT, et al. The total right/left-volume index: a new and simplified cardiac magnetic resonance measure to evaluate the severity of Ebstein anomaly of the tricuspid valve: a comparison with heart failure markers from various modalities. Circ Cardiovasc Imaging. 2014;7(4):601–9.

23. Etoom Y, Govindapillai S, Hamilton R, et al. Importance of CMR within the Task Force Criteria for the diagnosis of ARVC in children and adolescents. J Am Coll Cardiol. 2015;65(10):987–95.

24. Marcus FI, McKenna WJ, Sherrill D, et al. Diagnosis of arrhythmogenic right ventricular cardiomyopathy/dysplasia: proposed modification of the task force criteria. Circulation. 2010;121(13):1533–41.

25. Wald RM, Haber I, Wald R, Valente AM, Powell AJ, Geva T. Effects of regional dysfunction and late gadolinium enhancement on global right ventricular function and exercise capacity in patients with repaired tetralogy of Fallot. Circulation. 2009;119(10):1370–7.

26. Zhong L, Gobeawan L, Su Y, et al. Right ventricular regional wall curvedness and area strain in patients with repaired tetralogy of Fallot. Am J Physiol Heart Circ Physiol. 2012;302(6):H1306–16.

27. Lytrivi ID, Ko HH, Srivastava S, et al. Regional differences in right ventricular systolic function as determined by cine magnetic resonance imaging after infundibulotomy. Am J Cardiol. 2004;94(7):970–3.

28. Bodhey NK, Beerbaum P, Sarikouch S, et al. Functional analysis of the components of the right ventricle in the setting of tetralogy of Fallot. Circ Cardiovasc Imaging. 2008;1(2):141–7.

29. Alghamdi MH, Mertens L, Lee W, Yoo SJ, Grosse-Wortmann L. Longitudinal right ventricular function is a better predictor of right ventricular contribution to exercise performance than global or outflow tract ejection fraction in tetralogy of Fallot: a combined echocardiography and magnetic resonance study. Eur Heart J Cardiovasc Imaging. 2013;14(3):235–9.

30. Bove T, Vandekerckhove K, Devos D, et al. Functional analysis of the anatomical right ventricular components: should assessment of right ventricular function after repair of tetralogy of Fallot be refined? Eur J Cardiothorac Surg. 2014;45(2):e6–12.

31. Lee CM, Sheehan FH, Bouzas B, Chen SS, Gatzoulis MA, Kilner PJ. The shape and function of the right ventricle in Ebstein's anomaly. Int J Cardiol. 2013;167(3):704–10.

32. Johansson B, Babu-Narayan SV, Kilner PJ. The effects of breath-holding on pulmonary regurgitation measured by cardiovascular magnetic resonance velocity mapping. J Cardiovasc Magn Reson. 2009;11:1.

33. Gorter TM, van Melle JP, Freling HG, et al. Pulmonary regurgitant volume is superior to fraction using background-corrected phase contrast MRI in determining the severity of regurgitation in repaired tetralogy of Fallot. Int J Cardiovasc Imaging. 2015;31(6):1169–77.

34. Wald RM, Redington AN, Pereira A, et al. Refining the assessment of pulmonary regurgitation in adults after tetralogy of Fallot repair: should we be measuring regurgitant fraction or regurgitant volume? Eur Heart J. 2009;30(3):356–61.

35. O'Brien KR, Cowan BR, Jain M, Stewart RA, Kerr AJ, Young AA. MRI phase contrast velocity and flow errors in turbulent stenotic jets. J Magn Reson Imaging. 2008;28(1):210–8.

36. Burk J, Blanke P, Stankovic Z, et al. Evaluation of 3D blood flow patterns and wall shear stress in the normal and dilated thoracic aorta using flow-sensitive 4D CMR. J Cardiovasc Magn Reson. 2012;14:84.

37. Rutz T, Meierhofer C, Naumann S, et al. Comparison of MR flow quantification in peripheral and main pulmonary arteries in patients after right ventricular outflow tract surgery: A retrospective study. J Magn

Reson Imaging. 2017. doi: https://doi.org/10.1002/jmri.25701 [Epub ahead of print].

38. Pedrizzetti G, Claus P, Kilner PJ, Nagel E. Principles of cardiovascular magnetic resonance feature tracking and echocardiographic speckle tracking for informed clinical use. J Cardiovasc Magn Reson. 2016;18(1):51.

39. Tee M, Noble JA, Bluemke DA. Imaging techniques for cardiac strain and deformation: comparison of echocardiography, cardiac magnetic resonance and cardiac computed tomography. Expert Rev Cardiovasc Ther. 2013;11(2):221–31.

40. Ohyama Y, Ambale-Venkatesh B, Chamera E, et al. Comparison of strain measurement from multimodality tissue tracking with strain-encoding MRI and harmonic phase MRI in pulmonary hypertension. Int J Cardiol. 2015;182:342–8.

41. Shehata ML, Harouni AA, Skrok J, et al. Regional and global biventricular function in pulmonary arterial hypertension: a cardiac MR imaging study. Radiology. 2013;266(1):114–22.

42. Kim D, Gilson WD, Kramer CM, Epstein FH. Myocardial tissue tracking with two-dimensional cine displacement-encoded MR imaging: development and initial evaluation. Radiology. 2004;230(3):862–71.

43. Auger DA, Zhong X, Epstein FH, Spottiswoode BS. Mapping right ventricular myocardial mechanics using 3D cine DENSE cardiovascular magnetic resonance. J Cardiovasc Magn Reson. 2012;14:4.

44. Hor KN, Baumann R, Pedrizzetti G, et al. Magnetic resonance derived myocardial strain assessment using feature tracking. J Vis Exp. 2011;(48):pii: 2356.

45. Kempny A, Fernandez-Jimenez R, Orwat S, et al. Quantification of biventricular myocardial function using cardiac magnetic resonance feature tracking, endocardial border delineation and echocardiographic speckle tracking in patients with repaired tetralogy of Fallot and healthy controls. J Cardiovasc Magn Reson. 2012;14:32.

46. Lu JC, Ghadimi Mahani M, Agarwal PP, Cotts TB, Dorfman AL. Usefulness of right ventricular free wall strain to predict quality of life in "repaired" tetralogy of Fallot. Am J Cardiol. 2013;111(11):1644–9.

47. Moon TJ, Choueiter N, Geva T, Valente AM, Gauvreau K, Harrild DM. Relation of biventricular strain and dyssynchrony in repaired tetralogy of fallot measured by cardiac magnetic resonance to death and sustained ventricular tachycardia. Am J Cardiol. 2015;115(5):676–80.

48. Orwat S, Diller GP, Kempny A, et al. Myocardial deformation parameters predict outcome in patients with repaired tetralogy of Fallot. Heart. 2016;102(3):209–15.

49. Mahrholdt H, Wagner A, Judd RM, Sechtem U. Assessment of myocardial viability by cardiovascular magnetic resonance imaging. Eur Heart J. 2002;23(8):602–19.

50. Grosse-Wortmann L, Macgowan CK, Vidarsson L, Yoo SJ. Late gadolinium enhancement of the right ventricular myocardium: is it really different from the left? J Cardiovasc Magn Reson. 2008;10:20.

51. Larose E, Ganz P, Reynolds HG, et al. Right ventricular dysfunction assessed by cardiovascular magnetic resonance imaging predicts poor prognosis late after myocardial infarction. J Am Coll Cardiol. 2007;49(8):855–62.

52. Chen CA, Dusenbery SM, Valente AM, Powell AJ, Geva T. Myocardial ecv fraction assessed by CMR is associated with type of hemodynamic load and arrhythmia in repaired tetralogy of Fallot. JACC Cardiovasc Imaging. 2016;9(1):1–10.

53. Mehta BB, Chen X, Bilchick KC, Salerno M, Epstein FH. Accelerated and navigator-gated look-locker imaging for cardiac T1 estimation (ANGIE): development and application to T1 mapping of the right ventricle. Magn Reson Med. 2015;73(1):150–60.

54. Hartke LP, Gilkeson RC, O'Riordan MA, Siwik ES. Evaluation of right ventricular fibrosis in adult congenital heart disease using gadolinium-enhanced magnetic resonance imaging: initial experience in patients with right ventricular loading conditions. Congenit Heart Dis. 2006;1(5):192–201.

55. Kim H, Park EA, Lee W, et al. Magnetic resonance imaging findings of isolated right ventricular hypoplasia. Int J Cardiovasc Imaging. 2012;28(Suppl 2):149–52.

56. Riesenkampff E, Messroghli DR, Redington AN, Grosse-Wortmann L. Myocardial T1 mapping in pediatric and congenital heart disease. Circ Cardiovasc Imaging. 2015;8(2):e002504.

57. Chen CA, Tseng WY, Wang JK, et al. Circulating biomarkers of collagen type I metabolism mark the right ventricular fibrosis and adverse markers of clinical outcome in adults with repaired tetralogy of Fallot. Int J Cardiol. 2013;167(6):2963–8.

58. Jeewa A, Manickaraj AK, Mertens L, et al. Genetic determinants of right-ventricular remodeling after tetralogy of Fallot repair. Pediatr Res. 2012;72(4):407–13.

59. Rydman R, Gatzoulis MA, Ho SY, et al. Systemic right ventricular fibrosis detected by cardiovascular magnetic resonance is associated with clinical outcome, mainly new-onset atrial arrhythmia, in patients after atrial redirection surgery for transposition of the great arteries. Circ Cardiovasc Imaging. 2015;8(5):pii: e002628.

60. Babu-Narayan SV, Goktekin O, Moon JC, et al. Late gadolinium enhancement cardiovascular magnetic resonance of the systemic right ventricle in adults with previous atrial redirection surgery for transposition of the great arteries. Circulation. 2005;111(16):2091–8.

61. Plymen CM, Sado DM, Taylor AM, et al. Diffuse myocardial fibrosis in the systemic right ventricle of patients late after Mustard or Senning surgery: an equilibrium contrast cardiovascular magnetic resonance study. Eur Heart J Cardiovasc Imaging. 2013;14(10):963–8.

62. Babu-Narayan SV, Kilner PJ, Li W, et al. Ventricular fibrosis suggested by cardiovascular magnetic resonance in adults with repaired tetralogy of fallot and its relationship to adverse markers of clinical outcome. Circulation. 2006;113(3):405–13.

63. Park SJ, On YK, Kim JS, et al. Relation of fragmented QRS complex to right ventricular fibrosis detected by late gadolinium enhancement cardiac magnetic resonance in adults with repaired tetralogy of fallot. Am J Cardiol. 2012;109(1):110–5.

64. Broberg CS, Chugh SS, Conklin C, Sahn DJ, Jerosch-Herold M. Quantification of diffuse myocardial fibrosis and its association with myocardial dysfunction in congenital heart disease. Circ Cardiovasc Imaging. 2010;3(6):727–34.

65. Yim D, Riesenkampff E, Caro-Dominguez P, Yoo SJ, Seed M, Grosse-Wortmann L. Assessment of diffuse ventricular myocardial fibrosis using native t1 in children with repaired tetralogy of Fallot. Circ Cardiovasc Imaging. 2017;10(3):e005695.

66. Sato Y, Kato K, Hashimoto M, et al. Localized right ventricular structural abnormalities in patients with idiopathic ventricular fibrillation: magnetic resonance imaging study. Heart Vessel. 1996;11(2):100–3.

67. Roest AA, Kunz P, Lamb HJ, Helbing WA, van der Wall EE, de Roos A. Biventricular response to supine physical exercise in young adults assessed with ultrafast magnetic resonance imaging. Am J Cardiol. 2001;87(5):601–5.

68. La Gerche A, Claessen G, Dymarkowski S, et al. Exercise-induced right ventricular dysfunction is associated with ventricular arrhythmias in endurance athletes. Eur Heart J. 2015;36(30):1998–2010.

69. Parish V, Valverde I, Kutty S, et al. Dobutamine stress MRI in repaired tetralogy of Fallot with chronic pulmonary regurgitation: a comparison with healthy volunteers. Int J Cardiol. 2013;166(1):96–105.

70. Roest AA, Helbing WA, Kunz P, et al. Exercise MR imaging in the assessment of pulmonary regurgitation and biventricular function in patients after tetralogy of fallot repair. Radiology. 2002;223(1):204–11.

71. Luijnenburg SE, Mekic S, van den Berg J, et al. Ventricular response to dobutamine stress relates to the change in peak oxygen uptake during the 5-year follow-up in young patients with repaired tetralogy of Fallot. Eur Heart J Cardiovasc Imaging. 2014;15(2):189–94.

72. Robbers-Visser D, Jan Ten Harkel D, Kapusta L, et al. Usefulness of cardiac magnetic resonance imaging combined with low-dose dobutamine stress to detect an abnormal ventricular stress response in children and young adults after fontan operation at young age. Am J Cardiol. 2008;101(11):1657–62.

73. Tulevski II, Lee PL, Groenink M, et al. Dobutamine-induced increase of right ventricular contractility without increased stroke volume in adolescent patients with transposition of the great arteries: evaluation with magnetic resonance imaging. Int J Card Imaging. 2000;16(6):471–8.

74. Tops LF, Roest AA, Lamb HJ, et al. Intraatrial repair of transposition of the great arteries: use of MR imaging after exercise to evaluate regional systemic right ventricular function. Radiology. 2005;237(3):861–7.